TISSUE ENGINEERING: Part A
Volume 15, Number 9, 2009

DOI: 10.1089/ten.tea.2008.0284

Original Article

Characterization of Endothelial Basement Membrane Nanotopography in Rhesus Macaque as a Guide for Vessel Tissue Engineering

Sara J. Liliensiek, Ph.D.,[1] Paul Nealey, Ph.D.,[2] and Christopher J. Murphy, D.V.M., Ph.D.[1]

Basement membranes have many features that greatly influence vascular endothelial cell function, including a complex three-dimensional topography. As a first step in the design and development of vascular prosthetics, we undertook a thorough characterization of the topographic features of endothelial vascular basement membranes utilizing transmission electron microscopy and scanning electron microscopy. Specifically, we quantitatively analyzed the topographic features present in the aorta, carotid, saphenous, and inferior vena cava vessels in the rhesus macaque. Our results indicate that vascular basement membranes are composed of a complex meshwork consisting of pores and fibers in the submicron (100–1000 nm) and nanoscale (1–100 nm) range, consistent with what has previously been reported in basement membranes of other tissues. We found significant differences ($p < 0.05$) in basement membrane thickness and pore and fiber diameter depending on the location and physical properties of the vessel. These results have relevance to our fundamental understanding of vascular endothelial cell–matrix interactions in health and disease, evolving strategies in cell and tissue engineering and the design of cardiovascular prosthetic devices.

Introduction

Over 17.5 million people, worldwide, will die from some form of cardiovascular disease this year.[1,2] Vascular bypass with a patient's own tissue can be utilized to treat a range of cardiac disease; however, approximately 7% of patients do not have suitable vascular tissue for autologous grafting due to damage from disease.[3–6] To address this issue, alternatives to autologous tissue replacement have been developed, which include tissue-engineered prosthetic grafts. Synthetic vascular implants, including Dacron, expanded polytetrafluorothylene, or other polymers, have had limited success in replacing high-flow, large-diameter vessels.[7–10] Limitations of these vascular replacements include clinical complications involving immunologic response and calcium deposition, as well as their lack of growth potential.[11] In addition, synthetic grafts have not been successful for small vessel implants (<5 mm), which are particularly prone to thrombosis, resulting in complete occlusion of the graft.[12–14] Therefore, there is great need for innovation in the design and development of novel cardiovascular prosthetics to provide a successful long-term alternative for clinical use in humans.[15–18]

To circumvent some of the recurring issues in the design of vascular replacements, research is now focused on engineering *de novo* vascular tissue.

Essential characteristics of the native vessel need to be closely replicated in the prosthetic design, including proper durability, biocompatibility, tissue integrity, and optimal biochemical properties for cell proliferation and growth. The vascular replacement can be categorized into three separate, but equally important, components for consideration in the design of vascular tissue: growth conditions, the cell-type utilized to create the engineered tissue, and the scaffold design.[19,20] While each of these components are equally important, the biophysical environment provided by the scaffold greatly influences the cell behavior and ultimately the overall success and longevity of the engineered tissue.

Historically, reports dating back to the 1960s have emphasized the importance of the endothelial biophysical environment, including the basement membrane, in the normal homeostatic state of vascular tissue. Alterations in basement membrane components and size have been implicated as an important indicator of several disease states, including diabetes mellitus and other vascular pathologies, and most likely influence the biophysical features, including compliance and topography.[21–26] These studies support the proposition that the endothelial basement membrane is essential for normal homeostasis of the tissue and will influence the patency of engineered vascular replacements.

Although the biochemical components that comprise the vascular basement membrane have been well characterized

[1]Department of Surgical Sciences, School of Veterinary Medicine, University of Wisconsin–Madison, Madison, Wisconsin.
[2]Department of Chemical Engineering, School of Engineering, University of Wisconsin–Madison, Madison, Wisconsin.

(a mixture of constituents including elastin, collagen IV, enactin/nidogen, heparan-sulfate proteoglycans, and laminin[27–31]), the biophysical characterization of the endothelial basement membrane has yet to be thoroughly examined. Limited studies have sought to characterize the topography of the endothelial basement membrane, which include kidney,[32–35] and a single report qualitatively described the topographic features of the basement membrane associated with the bovine carotid artery.[34] From these studies, we know that the molecular components that comprise the endothelial basement membrane form a complex three-dimensional topography of pores and fibers that have been shown to impact cell shape, growth, migration, differentiation, and proliferation of endothelial cells.[36,37]

Despite these initial studies a thorough characterization of the topographic features of vascular endothelium has not been reported. To improve clinical efficacy of vascular grafts, we hypothesize that incorporation of biophysical cues, specifically topography and the thickness of the endothelial basement membrane, should be critical components included in optimization of future scaffold design.[7,38–40] To address, we have chosen to characterize basement membranes from a variety of anatomic sites along the vascular tree. In this study, we report the topographic features of basement membranes from the descending aorta, left common carotid, the left saphenous vein, and the inferior vena cava of the rhesus macaque. These anatomic sites were chosen for topographic analysis due to their importance in medical applications and involvement in cardiovascular disease. The detailed quantification of vascular endothelial basement membrane topography provides both a logical and critical starting point for the fabrication of biomaterials with biologically relevant feature sizes.

Materials and Methods

Animals

Vascular tissues were harvested from nine adult healthy rhesus macaques ranging in age from 5 to 15 years and included both male and female subjects. These animals were sacrificed for unrelated ocular studies, and vasculature was unaffected. Tissue samples were obtained from healthy rhesus macaques euthanized in accordance with NIH guidelines on Care and Use of Animals in Research in correlation with studies performed by other investigators (Wisconsin National Primate Research Center and the University of Wisconsin–Madison, Madison, WI). Immediately after euthanasia, vascular tissues were harvested from (1) the descending aorta, (2) the left common carotid, (3) the left saphenous vein, and (4) inferior vena cava. For transmission electron microscopy (TEM) a total sample number of $n = 6$ (aorta and carotid) and $n = 4$ (saphenous and inferior vena cava) and for scanning electron microscopy (SEM) $n = 5$ (aorta and carotid) and $n = 4$ (saphenous and vena cava) were utilized.

Tissue preparation

Harvested vessels were prepared following previously published protocols.[41–45] Immediately after euthanasia, samples were harvested, immersed, and flushed with 1× phosphate buffered saline (137 mM NaCl, 2.7 mM KCl, 4.3 mM Na_2HPO_4, and 1.47 mM KH_2PO_4) (1×PBS). To examine and quantitate the basement membrane features of several different vessel locations, we needed to optimize removal of the endothelial cells without compromising the integrity of the underlying basement membrane. The endothelium was removed by sonication. Specimens were placed in 15 mL conical tubes containing 1× PBS and immersed in a sonicator to mechanically displace endothelial cells from the basement membrane. The goal was to remove adequate numbers of endothelial cells to allow for imaging of the basement membrane. We delivered the lowest amount of energy possible to minimize the introduction of confounding artifacts. Optimized parameters for sonication that resulted in substantial removal of endothelium with preservation of the underlying basement membrane were 2 A delivered for 3 min, (Branson 3150®; Branson Ultrasonics BV, Eemnes, The Netherlands). Samples from both intact and denuded vessels were then immersion-fixed for 2 h at 4°C in Karnofsky's fixative (2% paraformaldehyde and 2% glutaraldehyde) for TEM and SEM or 4% paraformaldehyde–PBS for light microscopy (LM).

LM and immunohistochemistry

For LM, both intact and denuded vessel samples were rinsed in 1× PBS and submerged overnight in 20% sucrose–PBS in preparation for freezing. Tissues were frozen in Tissue-Tek OCT using isopentane cooled with liquid nitrogen. Frozen tissue was sectioned to a thickness of 6 μm and mounted on adhesive-coated aminosilane glass slides (Newcomer Supply, Madison, WI). Sections of vessels were stained with hematoxylin and eosin for evaluation of morphology. For immunohistochemical staining, tissue sections were placed in −20°C acetone for 5 min, dried, rinsed in 1× PBS, and blocked for 30 min in 3% normal goat serum (NGS)–PBS (Sigma-Aldrich, St. Louis, MO). Samples of aorta, carotid, saphenous, and vena cava were stained with 50 μL of a 1:40 dilution of rabbit antilaminin in 3% NGS-PBS for 1 h followed by a 30 min incubation in goat anti-rabbit (IgG) secondary antibody (Alexa Fluor® 594; Molecular Probes, Eugene, OR) at a concentration of 1:1000 in 3% NGS-PBS. In addition, sections were stained with 4′, 6-diamidino-2-phenylindole (DAPI; Invitrogen, Carlsbad, CA) to visualize cell nuclei. Each sample was imaged using an inverted fluorescence microscope equipped with rhodamine and DAPI filters (Axiovert 200M; Zeiss, New York, NY). Images were analyzed using Axiovision software.

Transmission electron microscopy

Specimens of de-endothelialized and control vessels were initially fixed at 4°C for 2 h with a modified Karnovsky's fixative (2.5% glutaraldehyde and 2% paraformaldehyde in 0.1 M Sorenson's Phosphate Buffer), rinsed in the same buffer, and then postfixed with 2% osmium tetroxide in 0.1 M Sorenson's PB. Next, the samples were dehydrated through a graded ethanol series (5 min each in 30%, 50%, 70%, 80%, 90%, and 100% and a final rinse for 10 min in absolute 100%), rinsed twice with propylene oxide, and then infiltrated with a 1:1 mixture of Polybed 812 and Spurr's epoxy resins (Polysciences, Warrington, PA) combined with an equal volume of propylene oxide. The samples were tightly covered and rotated in this mixture overnight at room temperature. The following day, the specimens were infiltrated with 100% resin mixture on a rotator at 60°C. The resin

mixture was exchanged at 45 min intervals for 4 h. Finally, the specimens were embedded in small aluminum weighing dishes and polymerized at 60°C for 24 h.

After polymerization, the samples were cut out of the molds and reoriented for sectioning. First, semithin sections (1 μm) were collected to insure proper orientation and structural integrity. Next, 60–90 nm sections were collected on 200 mesh copper grids for TEM observations. Sections were contrasted with uranyl acetate (a saturated solution of uranyl acetate in 50% EtOH) and Reynold's lead citrate. All sectioning was preformed with a Reichert Jung Ultracut E ultramicrotome. Photomicrographs of the endothelial basement membrane in cross section at several different magnifications were taken (CM120 TEM; Philips, Eindhoven, The Netherlands). For basement membrane thickness, five or more locations were imaged at 31,000× from each vessel sample. Five separate measurements were taken from each photomicrograph using AnalySIS FIVE software (Software Imaging System, Denver, CO). The mean and standard error (SEM) of the basement membrane thickness for aorta, carotid, saphenous, and inferior vena cava vessels were calculated.

Scanning electron microscopy

Samples from each vessel were dehydrated in graded alcohols (30–100%) followed by several 15 min exchanges in absolute alcohol, and critical-point dried in CO_2.[46] Samples were mounted on carbon stubs, and a 4 nm coating of platinum was then applied using an ion-beam sputter (VCR Group, San Clemente, CA). A low-voltage, high-resolution SEM (S-4700; Hitachi Scientific Instruments, Berkshire, England) or a LEO 15XX SEM (Leo Electron Microscopy, Cambridge, England) was used at 1–15 kV to capture images of the samples at various magnifications ranging from 1000× to 30,000×. Twelve random measurements from at least three separate micrographs on different locations of each vessel sample were taken at 30,000× to calculate pore and fiber diameter. Fiber and pore diameters were quantified using Image J software. Measurements were pooled, and a fiber and pore mean and SD were calculated.

Statistical analysis

The mean and standard error of the mean for basement membrane thickness (TEM) and pore and fiber diameter (SEM) were calculated as stated in previous sections. The measurements from samples for each vessel-type were compared using one-way analysis of variance. When analysis of variance was determined to be significant ($p < 0.05$), an unpaired t-test was utilized to determine significance ($p < 0.05$) between groups.

Results

We elected to perform morphologic studies primarily on nonhuman primates to eliminate possible confounding variables introduced by variations in donor age, state of health, and time to fixation intrinsic to the use of human cadaver tissues. Flushing of the vessels followed by sonication adequately removed endothelial cells while preserving the integrity of the basement membrane. Immunofluorescence staining for a known basement membrane component, laminin, was utilized to confirm presence of intact basement membrane after removal of the endothelium. In Figure 1 it can be seen that laminin expression and the endothelial cell nuclei were observed in control (A) and de-endothelialized (B) carotid samples. After sonication, endothelial cells have been displaced; however, laminin expression similar to that seen in the control untreated samples is still observed. Similar results were obtained for all other vascular tissues examined (data not shown). Our results indicate that the basement membrane integrity was preserved upon removal of the overlying endothelial cells.

Samples from rhesus macaque aorta, carotid, saphenous, and inferior vena cava were prepared for both SEM and TEM. With SEM (Fig. 2A, B), an endothelial cell can be seen attaching to the underlying stroma through the basement membrane. An area of low magnification was highlighted and magnified to display the basal aspect of the cell membrane adhering to the basement membrane.

We quantitated topographic features of the basement membrane from each vessel type. Figure 3 illustrates representative images of intact exposed basement membrane of each vessel type at both low (1000×) and high (30,000×) magnification. Each of the images documents the complex three-dimensional meshwork of pores and fibers in the nanometer range that is similar for each basement membrane vessel type.

To fully characterize the feature dimensions and size of the topographic features (pores and fibers) illustrated in

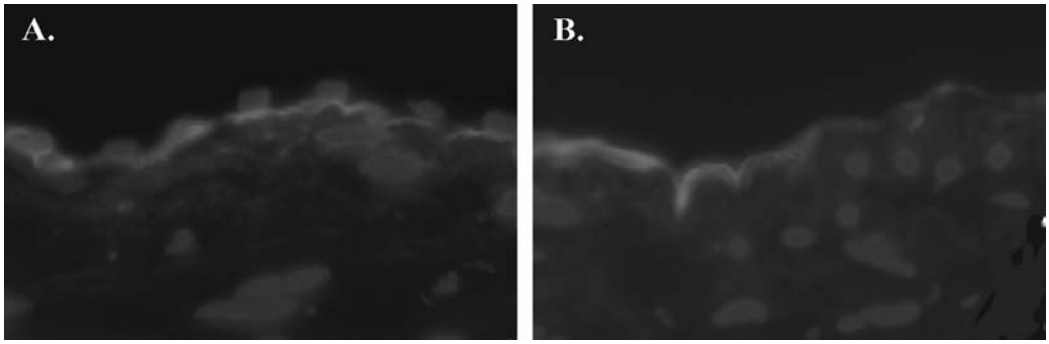

FIG. 1. Sonication results in adequate removal of endothelial cells with exposure of the basement membrane. Frozen sections of control and sonicated vessels were stained with an antilaminin antibody and DAPI to demonstrate removal of endothelial cells and preservation of basement membrane. (**A**) Untreated section of carotid tissue. (**B**) Sonicated carotid. All images were taken at 40×.

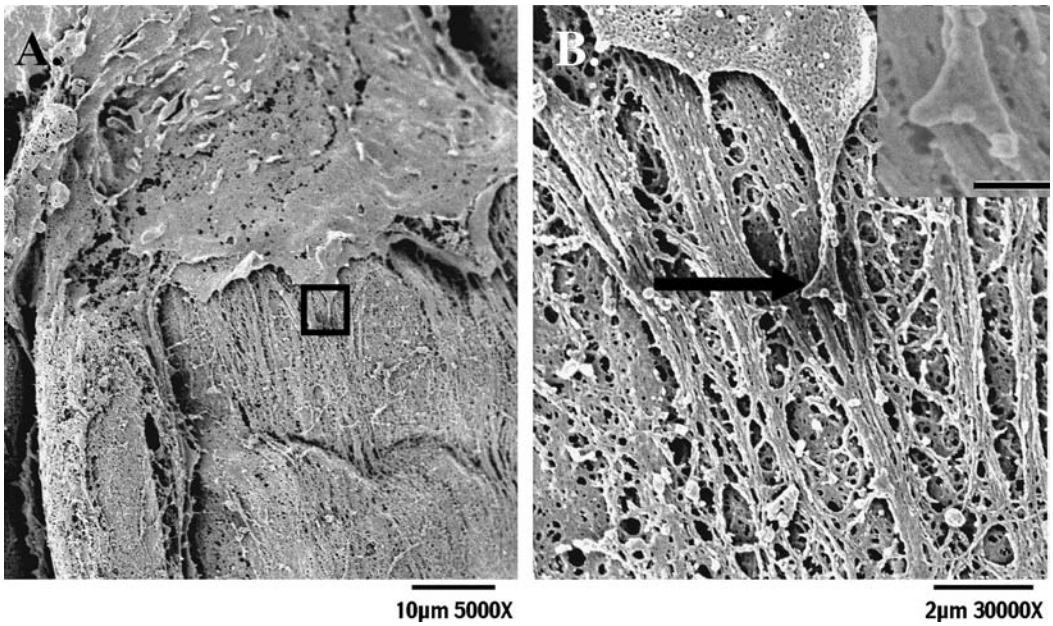

FIG. 2. Interaction of an aortic endothelial cell with the basement membrane in an intact vessel. (**A**) Low-magnification scanning electron micrographs of endothelial cell and basement membrane (scale bar = 3 μm). The black inset marks the area that is magnified in (**B**) (scale bar = 600 nm). In the inset in the upper right corner, scale bar = 200 nm.

Figure 3, we took additional SEM images to conduct measurements as previously described. The large arteries (aorta and carotid) had strikingly similar pore and fiber diameters as shown in Table 1. Both had pore diameters between 59 ± 4.5 and 63 ± 6 nm and fiber diameters between 31 ± 1 and 30 ± 2 nm. Relative to the arteries, both veins evaluated had a significantly smaller pore diameter average of 49 ± 2 and 38 ± 2 nm for the inferior vena cava and saphenous vein, respectively ($p < 0.0001$). The fiber diameter of both the inferior vena cava and saphenous vein were similar to the

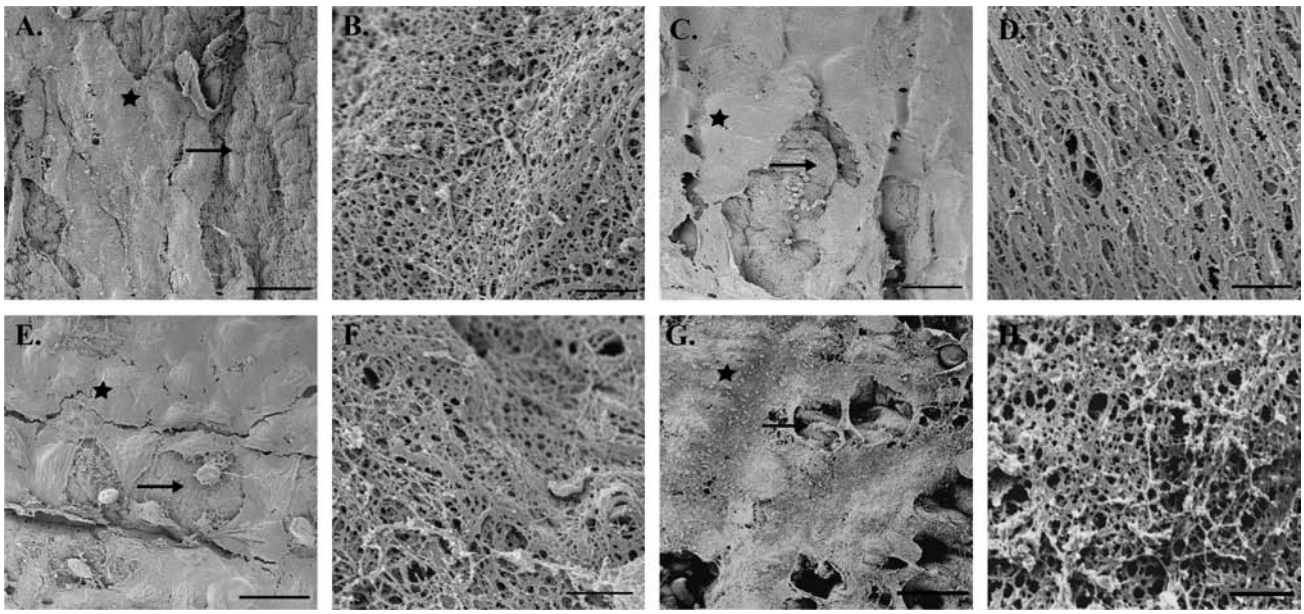

FIG. 3. Ultrastructural basement membrane architecture is broadly similar across vessel types. Scanning electron micrographs of the basement membranes from four separate vessels: aorta, carotid, saphenous, and inferior vena cava. Low-magnification images (1000 ×) exhibit areas of intact endothelium (star) and exposed basement membrane (arrow): (**A**) aorta (scale bar = 20 μm), (**C**) carotid (scale bar = 20 μm), (**E**) saphenous vein (scale bar = 20 μm), and (**G**) inferior vena cava (scale bar = 20 μm). High-magnification (30,000 ×) photomicrographs showing details of basement membrane topography: (**B**) aorta basement membrane (scale bar = 600 nm), (**D**) carotid basement membrane (scale bar = 600 nm), (**F**) saphenous vein basement membrane (scale bar = 600 nm), and (**H**) inferior vena cava basement membrane (scale bar = 600 nm).

Table 1. Calculation of Pore and Fiber Diameter for Rhesus Macaque Vasculature

Tissue	*Pore diameter (nm)*	*Fiber diameter (nm)*
Rhesus macaque aorta	59 ± 5	31 ± 1
Rhesus macaque carotid	63 ± 6	30 ± 2
Rhesus macaque saphenous	38 ± 2	27 ± 1
Rhesus macaque inferior vena cava	49 ± 2	24 ± 0.6
Porcine aortic valve[45]	38 ± 24	27 ± 12
Rhesus macaque cornea[42]	71 ± 44	77 ± 39
Human cornea[52]	92 ± 34	46 ± 16
Matrigel™[42]	105 ± 70	69 ± 35

The average pore and fiber diameters were calculated from aorta, carotid, saphenous vein, and inferior vena cava. Scanning electron micrographs were taken at 30,000×, and measurements were taken using Image J software. The mean and SEM were calculated. A one-way analysis of variance was used to determine significance between vessel pore size ($p < 0.05$). An unpaired *t*-test was used to determine significance between saphenous and both aorta and carotid ($p < 0.0001$) as well as inferior vena cava and aorta and carotid ($p < 0.0001$). Previously published values in the table represent the mean ± SD.

arteries at 24 ± 0.6 and 27 ± 1 nm. Table 1 includes the values for basement membrane topographic features from several different anatomic sites and species included for comparison. Our data indicate that the rhesus macaque vasculature has a complex nanotopography with similar feature types to other reported basement membranes. Quantitatively, the values found for the vascular basement membrane correspond broadly with reported nanoscale (1–100 nm) through submicron (100–1000 nm) values of pore diameter and fiber diameter taken from other species and anatomic sites (Table 1). However, we observed a decrease in pore and fiber diameter in our vascular samples when compared to most other tissue sites evaluated, with the exception of porcine aortic valve, indicating a more compact topographic surface.

Using TEM, we also investigated differences in overall basement membrane thickness between each of the vessels included in our studies. Initial qualitative observations of the different vessels indicate that there are variations in the thickness of the basement membranes. Upon qualitative examination of our images, the basement membrane of aorta appeared to have the thickest basement membrane. In addition, the basement membrane appeared loosely organized (Fig. 4A). Our images of carotid and inferior vena cava

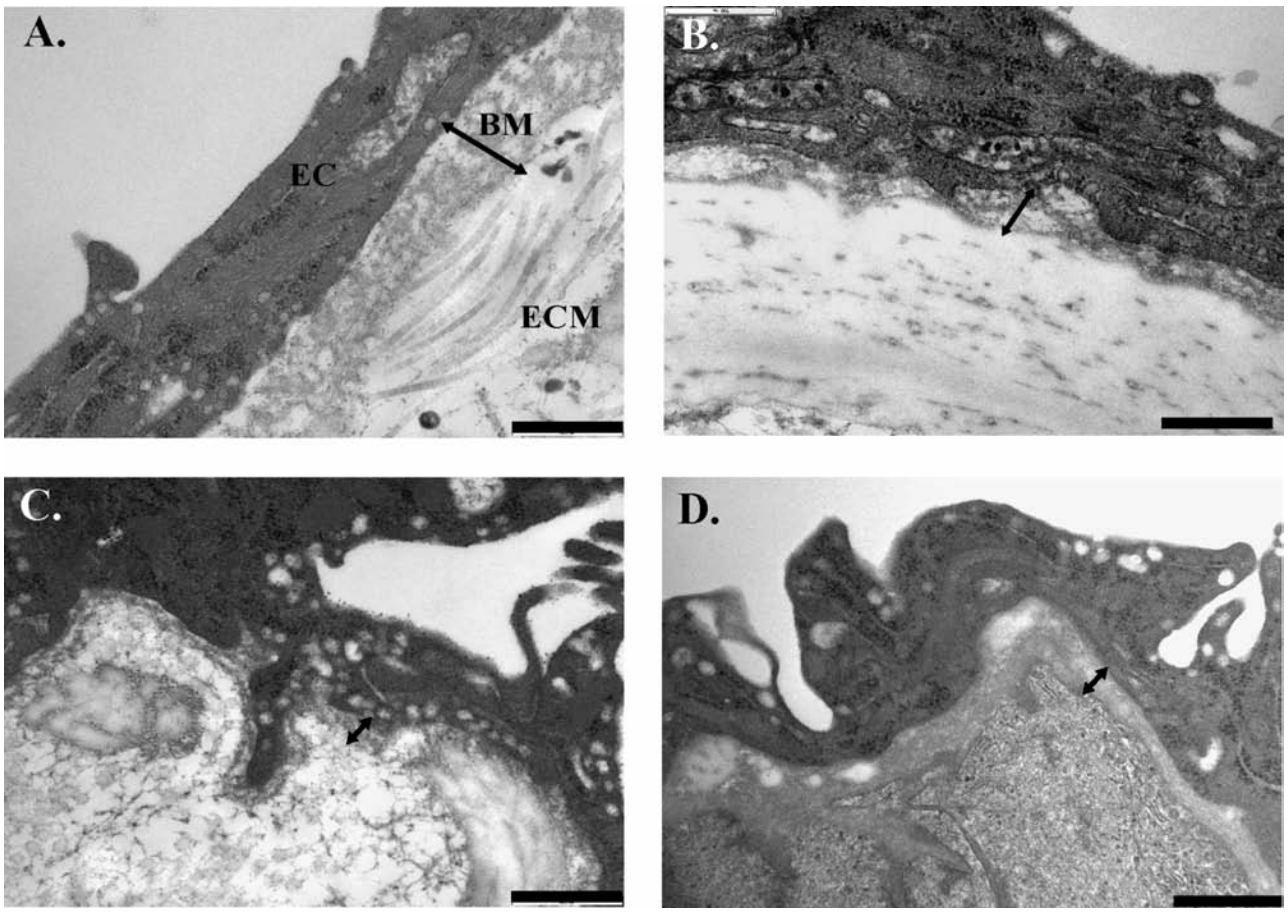

FIG. 4. Variations in basement membrane thickness and morphology across vessel types. The following transmission electron micrographs taken at 31,000× are representative of images utilized to determine basement membrane thickness. Cross sections of (**A**) aorta (scale bar = 500 nm), (**B**) carotid (scale bar = 500 nm), (**C**) saphenous (scale bar = 500 nm), and (**D**) inferior vena cava (scale bar = 500 nm) demonstrate the differences in basement membrane thickness and morphology across vessel types. BM, basement membrane; EC, endothelial cell; ECM, extracellular matrix.

basement membrane suggest that the basement membranes in these two locations are also amorphous, but thinner than what we observed for aortic tissue (Fig. 4B, D). Saphenous vein had a distinct, thin, and more easily identifiable basement membrane than observed for the other vessels (Fig. 4C).

Our TEM results suggest that there are differences in basement membrane thickness between vessels. We followed up this observation quantitatively by taking measurements of basement membrane thickness on each of our high-magnification (31,000×) transmission electron micrographs. Results detailing the average basement membrane thickness are shown in Figure 5. The mean basement membrane thickness of aorta was the greatest at $506 + 14$ nm. The rhesus macaque carotid and inferior vena cava tissue had lower averages of $319 + 14$ and $286 + 8.2$ nm. Saphenous had the lowest average of $112 + 8.2$ nm. We found statistically significant differences ($p < 0.05$) in thickness between several vessel types as indicated in Figure 5.

Discussion

This study represents our initial efforts to characterize the basement membrane topography and thickness of several clinically relevant vascular tissues for applied use in engineered scaffold design. In our investigation, we developed a novel approach to the removal of endothelial cells that we feel offers the advantage of being less disruptive than previously published methods, including dispase treatment,[47] N-heptanol,[48] mechanical dislodgement using air bubbles, or an EDTA rinse.[41–45,49] Although we do not achieve complete removal of the endothelial cells with sonication, the basement membrane that is exposed remains intact, as demonstrated by the presence of laminin immunofluorescence, as well as by SEM and TEM. Potential fixation[50] and dehydration[51]artifacts from processing tissues for SEM or TEM have been carefully considered and addressed in previous reports encompassing a range of different tissues (cornea, bladder, and aortic valve) and species (human, rhesus macaque, and canine), allowing us to measure the ultrastructural feature dimensions of the basement membrane.[41,45]

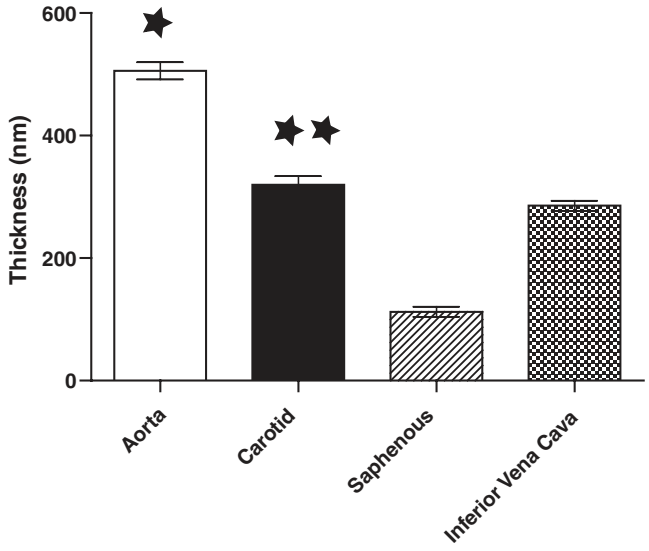

FIG. 5. Basement membrane thickness is significantly different across vessel types. Basement membrane thickness was calculated from transmission electron micrographs of each sample taken at 31,000×. Three separate areas from each tissue sample were imaged, and five random areas on each micrograph were measured. From the data, the mean and standard error of the mean were calculated. A one-way analysis of variance was used to determine the significance between groups ($p < 0.05$). An unpaired *t*-test was utilized to determine significance between selected comparisons (represented by asterisks). Significant differences were determined between aorta and saphenous ($p < 0.0001$), aorta and inferior vena cava ($p < 0.0001$), and carotid and saphenous ($p < 0.0001$).

Quantitative results obtained for the vascular endothelial basement membranes we examined broadly correspond with our previous reports of pore diameter and fiber diameter taken from other species and anatomic sites.[42,45,52] Aorta and carotid artery pore and fiber measurements were almost identical; however, the inferior vena cava and saphenous vein exhibited a significantly smaller pore diameter. Interestingly, the reduced pore diameter of the saphenous vein is similar to what has recently been reported in porcine aortic valve.[45] The heterogeneity of feature diameter measurements from different vessels may indicate critical differences that influence specific endothelial function for each vessel type.

Previous reports from our laboratory document that nanoscale features mimicking basement membrane feature sizes can promote changes in fundamental cell behaviors.[53] For many behaviors such as adhesion and proliferation, the ability to modulate these behaviors is not manifest until feature sizes approach the biomimetic size scale. For example, feature sizes less than 200 nm promote increased adhesion and decreased proliferation in human corneal epithelial cells.[54,55] These studies illustrate that differences in the structure of the biophysical environment may be involved in guiding cell behavior and the importance of characterizing the basement membrane features for future scaffold design.

In addition to the topographical analysis, we investigated changes in basement membrane thickness between vessels. Upon analysis we observed a great deal of variability both within vessel samples and between vessel types. Variations may be due to several different factors, including the species and vascular site reported,[56] the preparation and analysis of tissue,[57] or the physiological state of the tissue examined.[58,59] The endothelial basement membrane can also merge with the membranes of pericytes or smooth muscle cells or be absent in areas where projections from endothelial cells make contact with the aforementioned cell types, which also accounts for variability seen within each individual vessel type.[30,60–62] Historically, investigators had difficulty in identifying and quantitating measurements from the larger vessels that contain less defined, loosely arranged basement membrane zones when compared to smaller vessels such as capillaries.[60,61,63] At first, our quantitative results on the basement membrane thickness of the rhesus macaque aorta appeared to be twofold larger than what has been reported for other vascular tissues. However, several groups have also reported a wide basement membrane up to 900 nm in other larger vessels.[64,65] Results obtained for carotid, inferior vena cava, and saphenous were within the reported range of other vessel types.

Our results on vascular basement membrane thickness of normal tissue are important because most of the studies published on variations in thickness to date have focused on

vascular tissues in a diseased state. Examples include vessels found in tumors, changes in glomerular endothelial basement membrane in diabetes mellitus,[21,22,56,57] or vascular injury due to smoking[65] with significant thickening up to 5 μm in width of the basement membrane zones reported.[64,65] Changes in the thickness of the basement membrane zone most likely impact the physical features, including topography and compliance, which then in turn impacts the overlying endothelial cell behavior "tuning" it to a specific environmental niche or vessel type. Characterization of the normal basement membrane is therefore essential to begin to elucidate the impact of changes in the basement membrane, as it is related to a particular disease state and for the intelligent design of vascular replacements that can be applied in a variety of both normal and pathological circumstances.

Several groups have attempted to introduce native basement membrane into their design of vascular replacements. Decellularized veins from both canine and porcine models have been utilized as a scaffold.[66] Canine vessels that were denuded of cells had similar properties, including *in vitro* burst and suture holding, when compared to native intact vessels.[67] Amniotic membrane may also be considered a potential source for scaffolding material,[68] as it can serve as a scaffold for cell proliferation and differentiation, has antimicrobial and anti-immunogenic properties, and can be easily obtained. The overlying endothelial cells on the amniotic membrane exhibited more *in vivo*–like endothelial markers when compared to growth conditions on tissue culture plastic. These markers include enhanced platelet-endothelial cell adhesion molecule 1, adhesion molecule VE-cadherin at the intercellular junctions, and increased β1 integrin.[69] Although the results from all of the aforementioned studies are promising, these scaffolds still rely on acquisition of donated materials.

To avoid the use of donated tissue, researchers have sought to incorporate features of basement membranes, such as topography into their vascular replacement design. Ideally, the fabricated tissues provide environmental cues that mimic the basement membrane for vascular endothelial cell function. Promising results have been obtained using electrospun nanofibers from biological proteins, including silk fibroin, type I collagen, or elastin, which mimic the feature sizes of basement membrane observed *in vivo*.[70–76] For example, human aortic endothelial cells plated onto fibrous scaffolds (containing fibers in the range of 170 to 890 nm) exhibited cell-specific markers as measured by VE-cadherin, PECAM-1, von Willebrand Factor, normal proliferation, and formation of extracellular matrix. Other basement membrane components have been incorporated into scaffold design by modifying polypeptide from yeast translation termination factor protein that can self-assemble into nanofibers and improve endothelial cell adhesion. The result of this process yields a porous hydrogel that has been used as a coating material for vascular tissue.[77]

Despite all of the work mentioned attempting to incorporate basement membrane characteristics into the scaffold design, they have all taken a one-size-fits-all approach. None of the previously mentioned reports have characterized the biophysical features of the basement membrane of the specific vessel they are attempting to replace. The subtle variations in topography and thickness observed demonstrate the heterogeneity that exists between the biophysical features of basement membrane between large and small vessels. Incorporating the physical features of basement membrane, we have successfully measured in this report could enhance vessel strength, stability, patency, and overall success by providing appropriate environmental and organizational cues for cells within the vascular replacement.

We believe that our data on nanotopographic features and basement membrane thickness provide a rational starting point for the design and fabrication of biomaterials with biomimetic surface features. Our goal is to design substrates that mimic the nanoscale to submicron surface features present in native vascular endothelial basement membranes to study the interaction of vascular endothelial cells with topographic features. Our hope is that these studies will lead to a better understanding of the interplay between endothelial cells and their native basement membrane. In addition, the results of these studies will contribute to the development of novel strategies in cell and tissue engineering and will advance the development of cardiovascular prosthetics.

Acknowledgments

Sincere thanks to Dr. Paul Kaufman and the Wisconsin National Primate Research Center for providing us with the rhesus macaque tissue specimens needed for our studies; Ben August, Randall Massey, and Carolyn Smith for all of their expertise and assistance with TEM sample preparation and photomicrographs (Electron Microscopy Facility, University of Wisconsin–Madison); Phil Oshel and Dr. Ralph Albrecht for their assistance with SEM (University of Wisconsin–Madison); and Dr. Robert Auerbach (Department of Zoology University of Wisconsin–Madison) for constructive criticism of the manuscript. This research was funded by NSF-MRSEC, NIH-HL079012-01A, and #5P51RR000167.

Disclosure Statement

No competing financial interests exist.

References

1. World Health Organization. Fact Sheet 317: Cardiovascular Diseases. Geneva: World Health Organization, 2007.
2. American Heart Association. International Cardiovascular Disease Statistics, 2008, www.americanheart.org/presenter.jhtml?identifier-3001008.
3. Campbell, G.R., and Campbell, J.H. Development of tissue engineered vascular grafts. Curr Pharm Biotechnol **8,** 43, 2007.
4. Piccone, V. Modern Vascular Grafts. New York: McGraw-Hill, 1987.
5. Darling, R.C., and Linton, R.R. Durability of femoropopliteal reconstructions. Endarterectomy versus vein bypass grafts. Am J Surg **123,** 472, 1972.
6. Michaels, A.D., and Chatterjee, K. Cardiology patient pages. Angioplasty versus bypass surgery for coronary artery disease. Circulation **106,** e187, 2002.
7. Zhang, W.J., Liu, W., Cui, L., and Cao, Y. Tissue engineering of blood vessel. J Cell Mol Med **11,** 945, 2007.
8. Greisler, H.P. Interactions at the blood/material interface. Ann Vasc Surg **4,** 98, 1990.
9. Whittemore, A.D., Kent, K.C., Donaldson, M.C., Couch, N.P., and Mannick, J.A. What is the proper role of polytetrafluoroethylene grafts in infrainguinal reconstruction? J Vasc Surg **10,** 299, 1989.

10. Faries, P.L., Logerfo, F.W., Arora, S., Hook, S., Pulling, M.C., Akbari, C.M., Campbell, D.R., and Pomposelli, F.B., Jr. A comparative study of alternative conduits for lower extremity revascularization: all-autogenous conduit versus prosthetic grafts. J Vasc Surg **32,** 1080, 2000.
11. Kirklin, J.W., and Barratt-Boyes, B.G. Ventricular septal defect and pulmonary stenosis or atresia. In: Kirklin, J.W., and Barratt-Boyes, B.G., eds. Cardiac Surgery. New York: Churchill Livingstone, 1993, pp. 861–1612.
12. Pomposelli, F.B., Jr., Arora, S., Gibbons, G.W., Frykberg, R., Smakowski, P., Campbell, D.R., Freeman, D.V., and LoGerfo, F.W. Lower extremity arterial reconstruction in the very elderly: successful outcome preserves not only the limb but also residential status and ambulatory function. J Vasc Surg **28,** 215, 1998.
13. Clayson, K.R., Edwards, W.H., Allen, T.R., and Dale, A. Arm veins for peripheral arterial reconstruction. Arch Surg **111,** 1276, 1976.
14. Nerem, R.M., and Seliktar, D. Vascular tissue engineering. Annu Rev Biomed Eng **3,** 225, 2001.
15. Couet, F., Rajan, N., and Mantovani, D. Macromolecular biomaterials for scaffold-based vascular tissue engineering. Macromol Biosci **7,** 701, 2007.
16. Zidi, M., and Cheref, M. Mechanical analysis of a prototype of small diameter vascular prosthesis: numerical simulations. Comput Biol Med **33,** 65, 2003.
17. Seifalian, A.M., Tiwari, A., Hamilton, G., and Salacinski, H.J. Improving the clinical patency of prosthetic vascular and coronary bypass grafts: the role of seeding and tissue engineering. Artif Organs **26,** 307, 2002.
18. Kannan, R.Y., Salacinski, H.J., Butler, P.E., Hamilton, G., and Seifalian, A.M. Current status of prosthetic bypass grafts: a review. J Biomed Mater Res B Appl Biomater **74,** 570, 2005.
19. Riha, G.M., Lin, P.H., Lumsden, A.B., Yao, Q., and Chen, C. Review: application of stem cells for vascular tissue engineering. Tissue Eng **11,** 1535, 2005.
20. Bell, E. Tissue engineering in perspective. In: Lanza, R., Langer, R., and Vacanti, J., eds. Principles of Tissue Engineering. San Diego: Academic Press, 2000, pp. 35–40.
21. Siperstein, M.D., Unger, R.H., and Madison, L.L. Studies of muscle capillary basement membranes in normal subjects, diabetic, and prediabetic patients. J Clin Invest **47,** 1973, 1968.
22. Hayden, M.R., Sowers, J.R., and Tyagi, S.C. The central role of vascular extracellular matrix and basement membrane remodeling in metabolic syndrome and type 2 diabetes: the matrix preloaded. Cardiovasc Diabetol **4,** 9, 2005.
23. Magro, C.M., Calomeni, E.P., Nadasdy, T., Shusterman, B.D., Pope-Harman, A.L., and Ross, P., Jr. Ultrastructure as a diagnostic adjunct in the evaluation of lung allograft biopsies. Ultrastruct Pathol **29,** 95, 2005.
24. Baluk, P., Morikawa, S., Haskell, A., Mancuso, M., and McDonald, D.M. Abnormalities of basement membrane on blood vessels and endothelial sprouts in tumors. Am J Pathol **163,** 1801, 2003.
25. Simionescu, M., and Antohe, F. Functional ultrastructure of the vascular endothelium: changes in various pathologies. Handb Exp Pharmacol **176,** 41, 2006.
26. Tsilibary, E.C. Microvascular basement membranes in diabetes mellitus. J Pathol **200,** 537, 2003.
27. Yurchenco, P.D., and O'Rear, J. Supramolecular organization of basement membranes. In: Rohrbach, D.H., and Timpl, R., eds. Molecular and Cellular Aspects of Basement Membranes. San Diego: Academic Press, 1993, pp. 19–47.
28. Iivanainen, E., Kahari, V.M., Heino, J., and Elenius, K. Endothelial cell-matrix interactions. Microsc Res Tech **60,** 13, 2003.
29. Ekblom, E., and Timpl, R. Cell to cell contact and extracellular matrix, a multifaceted approach emerging. Curr Opin Cell Biol **8,** 599, 1996.
30. Timpl, R., and Aumailley, M. Biochemistry of basement membranes. Adv Nephrol Necker Hosp **18,** 59, 1989.
31. Martin, G.R., Timpl, R., and Kuhn, K. Basement membrane proteins: molecular structure and function. Adv Protein Chem **39,** 1, 1988.
32. Kubosawa, H., and Kondo, Y. Quick-freeze, deep-etch studies of the renal basement membrane. Microsc Res Tech **28,** 2, 1994.
33. Ruben, G.C., and Yurchenco, P.D. High resolution platinum-carbon replication of freeze dried basement membrane. Microsc Res Tech **28,** 13, 1994.
34. Murphy, C.J., and Goodman, S.L. Nano-scale replication of the extracellular matrix underlying the anterior corneal epithelium of the primate. Invest Ophthalmol Vis Sci S101, **37,** 1996.
35. Yamasaki, Y., Makino, H., and Ota, Z. Meshwork structures in bovine glomerular and tubular basement membrane as revealed by ultra-high-resolution scanning electron microscopy. Nephron **66,** 189, 1994.
36. Streuli, C., and Bissel, M.J. Expression of extracellular matrix components is regulated by substratum. J Cell Biol **110,** 1405, 1990.
37. Blake, D.A., Yu, H., Young, D.L., and Caldwell, D.R. Matrix stimulates the proliferation of human corneal endothelial cells in culture. Invest Ophthalmol Vis Sci **38,** 1119, 1997.
38. Francis, M.E., Uriel, S., and Brey, E.M. Endothelial cell-matrix interactions in neovascularization. Tissue Eng B Rev **14,** 19, 2008.
39. Pedersen, J.A., and Swartz, M.A. Mechanobiology in the third dimension. Ann Biomed Eng **33,** 1469, 2005.
40. Stegemann, J.P., Kaszuba, S.N., and Rowe, S.L. Review: advances in vascular tissue engineering using protein-based biomaterials. Tissue Eng **13,** 2601, 2007.
41. Abrams, G., Teixeria, A., Nealey, P., and Murphy, C. The effects of substratum topography on cell behavior. In: Dillow, A., and Lowman, A., eds. Biomimetic Materials and Design: Interactive Biointerfacial Strategies, Tissue Engineering, and Drug Delivery. New York: Marcel Dekker, 2002, pp. 91–136.
42. Abrams, G.A., Goodman, S.L., Nealey, P.F., Franco, M., and Murphy, C.J. Nanoscale topography of the basement membrane underlying the corneal epithelium of the rhesus macaque. Cell Tissue Res **299,** 39, 2000.
43. Abrams, G.A., Goodman, S.L., Nealey, P.F., and Murphy, C.J. Nanoscale topography of the extracellular matrix underlying the corneal epithelium of the non-human primate. Invest Ophthalmol Vis Sci **38,** s505, 1997.
44. Murphy, C.J., Abrams, G.A., Goodman, S.L., and Nealey, P.F. Nanoscale topographic features of basement membranes. Exp Eye Res **67,** 375, 1998.
45. Brody, S., Anilkumar, T., Liliensiek, S., Last, J.A., Murphy, C.J., and Pandit, A. Characterizing nanoscale topography of the aortic heart valve basement membrane for tissue engineering heart valve scaffold design. Tissue Eng **12,** 413, 2006.
46. Maser, M.D., and Trimble, J.J., III. Rapid chemical dehydration of biologic samples for scanning electron microscopy using 2,2-dimethoxypropane. J Histochem Cytochem **25,** 247, 1977.

47. Spurr, S.J., and Gipson, I.K. Isolation of corneal epitehlium with dispase II or EDTA. Invest Ophthalmol Vis Sci **26,** 818, 1985.
48. Cintron, C., Hassinge, L., Kublin, C., and Friend, J. A simple method for the removal of rabbit corneal epihelium utilizing n-heptanol. Ophthalmic Res **11,** 90, 1979.
49. Teixeira, A.I., McKie, G.A., Foley, J.D., Bertics, P.J., Nealey, P.F., and Murphy, C.J. The effect of environmental factors on the response of human corneal epithelial cells to nanoscale substrate topography. Biomaterials **27,** 3945, 2006.
50. Elder, H. Cryofixation. In: Bullock, G., and Pretusz, P., eds. Techniques in Immunocyochemistry. San Diego: Academic Press, 1989, pp. 1–28.
51. Hayat, M. Principles and Techniques of Electron Microscopy. New York: Van Nostrand Reinhold Co., 1970.
52. Abrams, G.A., Schaus, S.S., Goodman, S.L., Nealy, P.F., and Murphy, C.J. Nanoscale topography of the corneal epithelial basement membrane and descemet's membrane of the human. Cornea **19,** 57, 2000.
53. Gasiorowski, J.Z., Foley, J.D., Russell, P., Liliensiek, S.J., Nealey, P.F., and Murphy, C.J. Cellular behavior on basement membrane inspired topographically patterned synthetic matrices. In: Nair, L., ed. Biomedical Nanostructures. New York: John Wiley & Sons, Inc., 2007, pp. 297–319.
54. Liliensiek, S.J., Schell, K., Howard, E., Nealey, P., and Murphy, C.J. Cell sorting but not serum starvation is effective for SV40 human corneal epithelial cell cycle synchronization. Exp Eye Res **83,** 61, 2006.
55. Karuri, N.W., Liliensiek, S., Teixeira, A.I., Abrams, G., Campbell, S., Nealey, P.F., and Murphy, C.J. Biological length scale topography enhances cell-substratum adhesion of human corneal epithelial cells. J Cell Sci **117,** 3153, 2004.
56. Williamson, J.R., Vogler, N.J., and Kilo, C. Regional variations in the width of the basement membrane of muscle capillaries in man and giraffe. Am J Pathol **63,** 359, 1971.
57. Williamson, J.R., Vogler, N.J., and Kilo, C. Estimation of vascular basement membrane thickness. Theoretical and practical considerations. Diabetes **18,** 567, 1969.
58. Dockery, P., Khalid, J., Sarani, S.A., Bulut, H.E., Warren, M.A., Li, T.C., and Cooke, I.D. Changes in basement membrane thickness in the human endometrium during the luteal phase of the menstrual cycle. Hum Reprod Update **4,** 486, 1998.
59. Horbelt, D.V., Roberts, D.K., Parmley, T.H., and Walker, N.J. Ultrastructure of the microvasculature in human endometrial hyperplasia. Am J Obstet Gynecol **174,** 174, 1996.
60. Pease, D.C., and Paule, W.J. Electron microscopy of elastic arteries; the thoracic aorta of the rat. J Ultrastruct Res **3,** 469, 1960.
61. Gerrity, R.G., and Cliff, W.J. The aortic tunica intima in young and aging rats. Exp Mol Pathol **16,** 382, 1972.
62. Cliff, W.J. The extracellular components of blood vessel walls. In: Harrison, R.J., McMinn, R.M.H., and Treherne, J.E., eds. Blood Vessels. Cambridge: Cambridge University Press, 1976, pp. 97–124.
63. Parker, F. An electron microscope study of coronary arteries. Am J Anat **103,** 247, 1958.
64. Zweifach, B.W. Integrity of vascular endothelium. In: Altura, B.M., ed. Vascular Endothelium and Basement Membrane. New York: Karger, 1980, pp. 206–225.
65. Asmussen, I., and Kjeldsen, K. Intimal ultrastructure of human umbilical arteries. Observations on arteries from newborn children of smoking and nonsmoking mothers. Circ Res **36,** 579, 1975.
66. Wang, X., Lin, P., Yao, Q., and Chen, C. Development of small-diameter vascular grafts. World J Surg **31,** 682, 2007.
67. Schaner, P.J., Martin, N.D., Tulenko, T.N., Shapiro, I.M., Tarola, N.A., Leichter, R.F., Carabasi, R.A., and Dimuzio, P.J. Decellularized vein as a potential scaffold for vascular tissue engineering. J Vasc Surg **40,** 146, 2004.
68. Niknejad, H., Peirovi, H., Jorjani, M., Ahmadiani, A., Ghanavi, J., and Seifalian, A.M. Properties of the amniotic membrane for potential use in tissue engineering. Eur Cell Mater **15,** 88, 2008.
69. Tsai, S.H., Liu, Y.W., Tang, W.C., Zhou, Z.W., Hwang, C.Y., Hwang, G.Y., Ou, B.R., Hu, C.P., Yang, V.C., and Chen, J.K. Characterization of porcine arterial endothelial cells cultured on amniotic membrane, a potential matrix for vascular tissue engineering. Biochem Biophys Res Commun **357,** 984, 2007.
70. Soffer, L., Wang, X., Zhang, X., Kluge, J., Dorfmann, L., Kaplan, D.L., and Leisk, G. Silk-based electrospun tubular scaffolds for tissue-engineered vascular grafts. J Biomater Sci Polym Ed **19,** 653, 2008.
71. Zhang, X., Baughman, C.B., and Kaplan, D.L. *In vitro* evaluation of electrospun silk fibroin scaffolds for vascular cell growth. Biomaterials **29,** 2217, 2008.
72. Stitzel, J., Liu, J., Lee, S.J., Komura, M., Berry, J., Soker, S., Lim, G., Van Dyke, M., Czerw, R., Yoo, J.J., and Atala, A. Controlled fabrication of a biological vascular substitute. Biomaterials **27,** 1088, 2006.
73. Huang, L., Nagapudi, K., Apkarian, R.P., and Chaikof, E.L. Engineered collagen-PEO nanofibers and fabrics. J Biomater Sci Polym Ed **12,** 979, 2001.
74. Matthews, J.A., Wnek, G.E., Simpson, D.G., and Bowlin, G.L. Electrospinning of collagen nanofibers. Biomacromolecules **3,** 232, 2002.
75. Boland, E.D., Matthews, J.A., Pawlowski, K.J., Simpson, D.G., Wnek, G.E., and Bowlin, G.L. Electrospinning collagen and elastin: preliminary vascular tissue engineering. Front Biosci **9,** 1422, 2004.
76. Li, W.J., Laurencin, C.T., Caterson, E.J., Tuan, R.S., and Ko, F.K. Electrospun nanofibrous structure: a novel scaffold for tissue engineering. J Biomed Mater Res **60,** 613, 2002.
77. Xu, J., Zhou, X., Ge, H., Xu, H., He, J., Hao, Z., and Jiang, X. Endothelial cells anchoring by functionalized yeast polypeptide. J Biomed Mater Res A **87,** 819, 2008.

Address correspondence to:
Sara J. Liliensiek, Ph.D.
Department of Surgical Sciences
School of Veterinary Medicine
University of Wisconsin–Madison
2015 Linden Drive
Madison, WI 53706

E-mail: sjlilien@.wisc.edu

Received: May 15, 2008
Accepted: February 9, 2009
Online Publication Date: April 3, 2009